Elastic anisotropy of an $Fe_{79}Si_{12}B_9$ amorphous alloy thin film studied by ultrasound spectroscopy

Ryuichi Tarumi,[a] Akira Shibata, Hirotsugu Ogi, and Masahiko Hirao
Graduate School of Engineering Science, Osaka University, 1-3 Machikaneyama, Toyonaka, Osaka 560-8531, Japan

Kazuki Takashima
Department of Materials Science and Engineering, Kumamoto University, 2-39-1, Kurokami, Kumamoto 860-8555, Japan

Yakichi Higo
Precision and Intelligence Laboratory, Tokyo Institute of Technology, 4259 Nagatsuta, Yokohama, Kanagawa 226-8503, Japan

(Received 8 August 2006; accepted 30 December 2006; published online 12 March 2007)

A complete set of elastic constants C_{ij} of an $Fe_{79}Si_{12}B_9$ amorphous alloy free standing thin film has been determined by using ultrasound spectroscopy techniques. The out-of-plane shear moduli of C_{44} and C_{55} are measured by the thickness resonance frequencies and are almost elastic isotropic in the film plane indicating that the thin film has a hexagonal-type elastic symmetry. The remaining C_{ij} in the symmetry are determined by the modified resonance ultrasound spectroscopy coupled with a laser-Doppler interferometory. Inverse calculation showed elastic anisotropies between the in-plane and the out-of-plane directions; $C_{33}/C_{11}=1.21$ and $C_{66}/C_{44}=1.26$. Magnetic property measurements also revealed the remarkable magnetization difference between the two directions suggesting that the structural difference between the in-plane and the out-of-plane directions would be responsible for them. © *2007 American Institute of Physics*. [DOI: 10.1063/1.2538167]

I. INTRODUCTION

Because of the loss of long range ordering in their atomic configuration, ideal amorphous alloys have isotropic mechanical properties so that they are potential candidate material for the future application of microsized mechanical devices.[1] Generally, amorphous alloys are prepared by a rapid quenching technique by *freezing* the liquid structure into an ambient temperature. Most of amorphous alloys therefore show a thin film shape (micrometer-ordered thickness) to suppress the crystallization during the quenching process. Mechanical property measurement, especially complete set of elastic constants C_{ij} for amorphous alloy free standing thin films, is therefore an important issue for a reliable application to the micro-sized devices. Up to now, variety of C_{ij} measurement methods for free standing thin films has been developed, such as Brillouin scattering,[2–4] resonant vibration,[5,6] nanoindentation,[7] tensile test for microsized samples,[8,9] x-ray diffractions,[10] etc. These methods, however, give only one or two independent elastic constants so that one fails to consider elastic anisotropy of the thin films.

Resonant ultrasound spectroscopy (RUS) is an advanced technique to determine C_{ij} of an elastic medium.[11–15] This method determines all independent C_{ij} from free vibration resonance frequencies of a rectangular parallelepiped or spherical specimen with high accuracy. Application of RUS to free standing thin film, however, encounters the following problems:

(i) Conventional ultrasound transducers fail to detect resonance spectrum since resonance peak intensity is extremely low compared with those of mm^3-sized bulk specimen.
(ii) In principle, RUS fails to determine the out-of-plane shear moduli (C_{44} and C_{55}) since these components hardly affect the free vibration resonance frequencies of the thin film shaped materials.

Thus, RUS technique has not been applied to evaluate C_{ij} of a free standing thin film. In this study, we succeeded to overcome these problems by using electromagnetic acoustic resonance (EMAR) and modified RUS method which coupled with a laser-Doppler interferometer (RUS/LDI). Application of this technique to an Fe-based amorphous alloy free standing thin film shows finite elastic anisotropies between the in-plane and the out-of-plane directions both in the longitudinal and the shear components.

In the following section, we show the details of the thickness resonance of the EMAR method and the results of out-of-plane shear modulus. The remaining elastic constants are determined by using the modified RUS/LDI method in Sec. III. From these results, we discuss the origin of the elastic anisotropy in Sec. IV. Some concluding remarks are summarized in Sec. V.

II. ELECTROMAGNETIC ACOUSTIC RESONANCE

A. Experimental procedure

The material studied is an $Fe_{79}Si_{12}B_9$ (at. %) amorphous alloy thin film prepared by the single-roller rapid-quenching method. Crystalline phase has not been identified by x-ray

[a]Electronic mail: tarumi@me.es.osaka-u.ac.jp

diffraction measurement, conventional transmission electron microscopy (TEM) observation, and high-resolution TEM observation. To define the elastic constants C_{ij} of the amorphous alloy thin film, an $x_1-x_2-x_3$ Cartesian coordinate system has been employed. In the coordinate system, x_2 and x_3 are set to be the rolling direction and the film thickness direction, respectively. Average thickness and mass density of the specimen are 25.5 μm and 7039 kg/m^3, which were determined by cross-sectional scanning electron microscopy observation and by the Archimedes method, respectively.

As mentioned earlier, the out-of-plane shear moduli, such as C_{44} and C_{55}, are extremely insensitive to the free vibration resonance frequency of a thin film specimen so that RUS fails to determine them with sufficient accuracy. We have therefore employed a thickness resonance EMAR technique to determine the out-of-plane shear moduli prior to the RUS measurement.[16] The electromagnetic acoustic transducer (EMAT) is consisted of two parts; a pair of permanent magnets and an elongated spiral coil fixed at an end of the magnets. The EMAT is mounted on a surface of the specimen and the coil is droved by tone burst current (~60 MHz, 35 μs) to induce eddy currents near the specimen surface. The eddy currents and static magnetic field by the magnets interact to generate cyclic Lorentz forces, which turn into polarized shear wave traveling in the thickness direction (x_3-axis direction) of the thin film specimen. Here, the frequency of the shear wave corresponds to the driving burst currents and polarization direction depends on the direction of the elongated spiral coil.[16] Note that the EMAT detects the signals from shear wave through the reverse process. If the polarized shear wave satisfies the following relation, it becomes resonant state to the thickness direction

$$2d = nc/f_n, \quad (n = 1, 2, 3, \ldots), \tag{1}$$

where d, c, and f_n represent the specimen thickness, polarized shear wave velocity, and nth mode resonance frequency, respectively. Resonance frequencies f_n are determined from a frequency sweep using the EMAT. Here, out-of-plane shear moduli of C_{44} and C_{55} are obtained from polarized sound velocity c as follows:

$$c = \sqrt{C_{ij}/\rho}. \tag{2}$$

In the equation, ρ represents mass density of the specimen.

B. Experimental results

Figure 1(a) shows a thickness resonance EMAR spectrum obtained from the amorphous alloy thin film. The background noise is also shown in Fig. 1(b). In the spectrum (a), there is a bundle of sharp resonance peaks around 60 MHz. Since no peaks appeared in (b), and at low frequency side of (a), these peaks represent the fundamental mode shear wave resonance. The splitting of resonance peaks can be explained by the thickness fluctuation (1 MHz frequency fluctuation corresponds to a 400 nm thickness fluctuation). To eliminate this effect, we measured the thickness resonance EMAR spectrum at 20 different points. The obtained data are numerically averaged for respective polarization directions and we fit the Gaussian function to them by the least-square scheme. The center axis gives average resonance frequency of the mode, which yields the corresponding shear wave velocity and then the out-of-plane shear modulus from Eqs. (1) and (2).

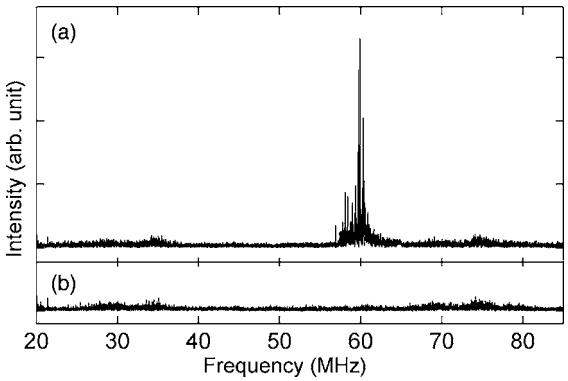

FIG. 1. (a) Thickness resonance EMAR spectrum and (b) corresponding background noise obtained by the FeSiB amorphous alloy free standing thin film. The bundle of resonance peaks around 60 MHz shows the first mode thickness resonance for polarized shear wave.

The out-of-plane shear moduli are determined as a function of polarization direction θ of the shear wave. Here, we set the θ from x_1 ($\theta=0$) to x_2 ($\theta=\pi/2$) axis direction with $\Delta\theta$ of $\pi/8$. Note that C_{55} and C_{44} are corresponding to $\theta=0$ and $\pi/2$, respectively. As a result, out-of-plane shear moduli increase with in creasing θ from $C_{55}=62.8$ GPa to $C_{44}=64.1$ GPa representing that the amorphous alloy thin film has elastic anisotropy. The deviation from isotropy is however very weak; anisotropy is only 3% between C_{55} and C_{44}. It is therefore reasonable to consider that the amorphous alloy thin film is elastically isotropic about the out-of-plane directions. Thus, we assume the following hexagonal-type elastic symmetry

$$C_{ij} = \begin{bmatrix} C_{11} & C_{12} & C_{13} & 0 & 0 & 0 \\ C_{12} & C_{11} & C_{13} & 0 & 0 & 0 \\ C_{13} & C_{13} & C_{33} & 0 & 0 & 0 \\ 0 & 0 & 0 & C_{44} & 0 & 0 \\ 0 & 0 & 0 & 0 & C_{44} & 0 \\ 0 & 0 & 0 & 0 & 0 & C_{66} \end{bmatrix}. \tag{3}$$

In the elastic symmetry, C_{ij} are invariant for any rotation about the x_3 axis and number of independent component is five: C_{11}, C_{33}, C_{23}, C_{66}, and C_{44} [$C_{66}=(C_{11}-C_{12})/2$]. Note that if the amorphous alloy thin film is elastically isotropic, $C_{11}=C_{33}$, $C_{12}=C_{13}$, $C_{44}=C_{66}$, and $C_{12}=C_{11}-2C_{44}$. In the following analysis, we set an average of $\theta=0$ and $\pi/2$ for out-of-plane shear modulus $C_{44}(=C_{55})$ in the hexagonal elastic symmetry. The remaining four elastic constants are determined by the modifying RUS/LDI technique.

III. RUS/LDI MEASUREMENT

A. Experimental procedure

Experimental set up for the RUS/LDI method is schematically illustrated in Fig. 2. A $4.45\times3.40\times0.0255$ mm^3 sized specimen is mechanically cut from the amorphous alloy sheet and mount on the tripod pinducers with a special

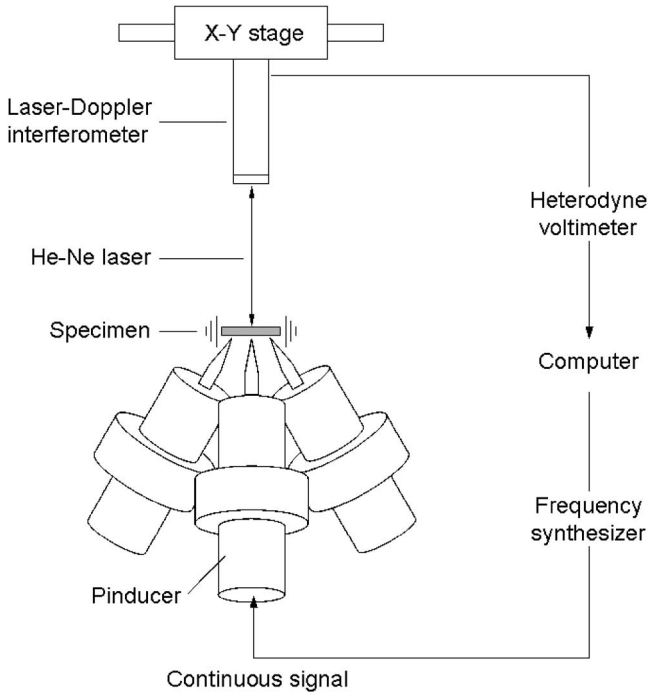

FIG. 2. A schematic illustration of an RUS/LDI measurement system. A He-Ne laser beam, focused on a surface of the specimen, detects the vibration amplitude as a function of the input ultrasound frequency.

care. In previous RUS/LDI method, one pinducer excites ultrasound vibration and another detects the vibration amplitude as a function of the input frequency. The free vibration resonance frequencies are then obtained by a frequency scan. In case of a free standing thin film, however, the conventional RUS method fails to obtain the resonance frequencies since the thin film specimen is extremely light so that the ultrasound transducer cannot detect clear vibration amplitude even in the resonance states because of the too weak acoustic coupling. We have therefore detected vibrational amplitude of the specimen using a laser-Doppler interferometer, instead of a pinducer. As shown in Fig. 2, one pinducer excites continuous ultrasound signal to the specimen from the bottom side. During the vibration, the laser-Doppler interferometer detects vibrational amplitude of the specimen surface as a function of the input frequency. Since the interferometer can only detect the vibration at the focused point, it would fail to detect a resonance peak if the measuring point is set at the vibration node. Thus, the measurements are carried out for different points in the specimen. For respective resonance modes, we also measured the vibration amplitude distribution on the specimen surface by scanning the laser-Doppler interferometer.[17] These experimentally measured vibrational patterns are compared with those of theoretical ones to achieve unambiguous mode identification.

B. Experimental results

Figure 3 shows a resonance spectrum obtained by the modified RUS/LDI method. While it shows broad resonance peaks, we can identify the resonance frequencies from the spectrum by measuring vibrational figures. Figures 4 show measured (upper) and calculated (lower) surface vibration

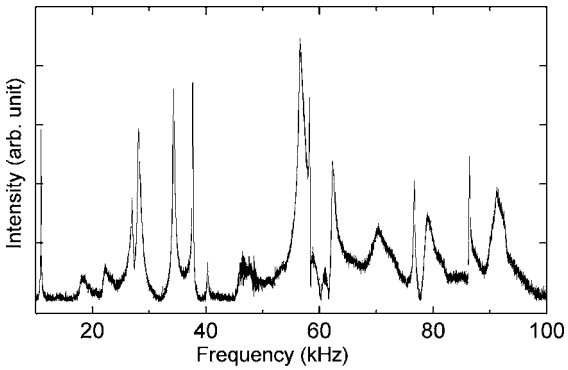

FIG. 3. Free vibration resonance spectrum of the amorphous alloy thin film obtained by modified RUS/LDI method. Resonance frequencies are determined by fitting the peaks using Gaussian function.

displacement distribution of $B_{1u}-5$, $B_{2g}-6$, and $B_{1u}-15$ resonant modes. As seen in the figures, all measured patterns show exact consistence with those calculated. Mode identification is therefore unambiguous and we inversely calculated the elastic constants from the resonance frequencies using the Rayleigh–Ritz method.

Table I shows the inverse calculation results. Here, df/dC_{ij} are called normalized contribution indicating the sensitivity of resonance frequencies to small variation of the elastic constants which obtained after the inverse calculation. Thus, high df/dC_{ij} yields accurate corresponding elastic constants. It should be emphasized that df/dC_{44} is remarkably small among any other df/dC_{ij}. In other words, kilohertz frequency-range resonance modes are insensitive to the out-of-plane shear modulus and this method fails to determine C_{44} with sufficient accuracy. In the present analysis, therefore, C_{44} is fixed to be an average of the EMAR results as mentioned earlier. Diff. in Table I represents the difference between measured and calculated resonance frequencies. The over all root-mean-square (rms) error becomes approximately 1.83% indicating that measurement accuracy of C_{ij} is approximately 3.7%.

IV. DISCUSSION

A. Elastic anisotropy

Table II summarizes a complete set of elastic constants of the FeSiB amorphous alloy thin film. Here, ν_{ij} stands for

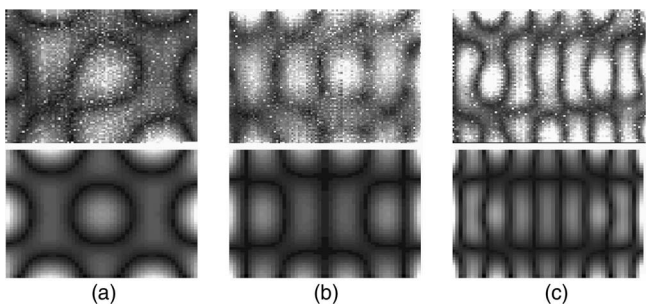

FIG. 4. Vibration displacement distributions for (a) $B_{1u}-5$, (b) $B_{2g}-6$, and (c) $B_{1u}-15$ resonance modes measured by the laser-Doppler interferometer. The black lines represent the vibration node and the antinode is shown in the white area. The measured (upper) and calculated (lower) patterns show excellent agreement.

TABLE I. Inverse calculation result for FeSiB arorphous alloy standing thin film measured by modified RUS/laser method. Diff. and df/dC_{ij} represent resonance frequency difference and contribution of elastic constants for respective vibration modes. Overall rms error becomes 1.8305%.

Mode	f^{Ex} (MHz)	f^{Cal} (MHz)	Diff. (%)	df/dC_{33}	df/dC_{23}	df/dC_{12}	df/dC_{44}	df/dC_{60}
$B_{2g}-3$	0.03738	0.03762	0.64	0.062	−0.123	0.221	0.003	0.838
$B_{2g}-4$	0.058526	0.057203	−2.26	0.105	−0.209	0.376	0.002	0.727
$B_{2g}-6$	0.077354	0.07836	1.3	0.089	−0.177	0.318	0.003	0.767
$B_{2g}-7$	0.087076	0.088936	2.14	0.091	−0.183	0.328	0.004	0.759
A_u-5	0.061957	0.063094	1.83	0.101	−0.202	0.363	0.002	0.735
$B_{1u}-5$	0.055788	0.055098	−1.24	0.071	−0.143	0.257	0.003	0.812
$B_{1u}-7$	0.073436	0.073033	−0.55	0.095	−0.19	0.34	0.003	0.751
$B_{1u}-8$	0.086382	0.086357	−0.03	0.119	−0.237	0.427	0.002	0.69
$B_{1u}-15$	0.181998	0.182505	0.28	0.109	−0.219	0.393	0.006	0.711
$B_{3g}-3$	0.041077	0.039735	−3.27	0.076	−0.153	0.274	0.002	0.8
$B_{3g}-5$	0.075997	0.078294	3.02	0.078	−0.156	0.279	0.004	0.795

an anisotropic Poisson's ratio indicating a contraction in the j direction under an uniaxial load in the i direction. In the hexagonal symmetry ν_{ij} can be expressed in the following form:

$$\nu_{12}=\frac{C_{33}C_{12}-C_{13}^2}{C_{33}C_{11}-C_{13}^2},\quad \nu_{13}=\frac{C_{13}C_{12}-C_{11}C_{13}}{C_{13}^2-C_{11}C_{33}},$$
$$\nu_{31}=\frac{C_{13}}{C_{11}+C_{12}}. \tag{4}$$

Note that $\nu_{12}=\nu_{21}$, $\nu_{13}=\nu_{23}$, and $\nu_{31}=\nu_{32}$. Using ν_{ij}, in-plane and out-of-plane Young's moduli of $E_{[100]}$ and $E_{[001]}$ are given by

$$E_{[100]}=(C_{11}-C_{12}\nu_{12}-C_{13}\nu_{13}),$$
$$E_{[001]}=(C_{33}-2C_{13}\nu_{31}). \tag{5}$$

Here, $E_{[100]}=E_{[010]}$. The bulk modulus B is given by the following relation:

$$B=\frac{(C_{11}+C_{12})C_{33}-2C_{13}^2}{C_{11}+C_{12}-4C_{13}+2C_{33}}. \tag{6}$$

In Table II, we included previous works for comparison with the present result.[18,19] The currently reported elastic constants of Fe-based amorphous alloy thin films are limited because of the difficulty on the precise elastic constants measurements, however, in-plane Young's modulus of this study becomes about the average of previous works and in-plane Poisson's ratio shows reasonable consistency.[18,19] Thus, the present results should be valid.

One of the significant observations found in this study is that the specimen shows elastic anisotropy regardless of its amorphous structure. Figure 5 summarizes the in-plane and out-of-plane elastic constants. As seen in the figure, elastic constants are deviated to the right side from the isotropic line indicating that the out-of-plane stiffnesses are higher than the in-plane stiffnesses both in compression and shear components. From Table II, the compression and shear anisotropies become $C_{33}/C_{11}=1.21$ and $C_{66}/C_{44}=1.26$. As mentioned earlier, measurement accuracy of elastic constants is approximately 3.7%. We have therefore concluded that the present results reveal elastic anisotropy between the in-plane and out-of-plane directions in the amorphous alloy thin film.

B. Magnetic property

The origin of elastic anisotropy in the amorphous alloy free standing thin film is also of our interest. In our previous structural analysis by TEM, mesoscopic structural inhomogeneity, such as microcrack or void, has not been confirmed. The atomistic scale anisotropy would therefore be one of the plausible reasons for the origin of this anisotropy. To clarify this point, we carried out magnetic property measurement for in-plane and out-of-plane directions using the superconducting quantum interference device (SQUID) at ambient temperature.

Figure 6 shows the magnetization curves obtained from the amorphous alloy thin film for in-plane (open circle) and out-of-plane (open triangle) magnetic field directions. Here, measurements are carried out up to 4×10^6 H. As shown in the figure, there are no hysteresis behaviors in both curves indicating that the amorphous alloy thin film has a remark-

TABLE II. Room temperature elastic constants of FeSiB amorphous alloy free standing thin film. The units are GPa for elastic constants C_{ij} , Young's modulus E, and bulk modulus B. ν_{ij} represents anisotropic Poisson's ratio indicating the contraction of the i direction under the uniaxial loading of the j direction.

	Reference	C_{11}	C_{33}	C_{13}	C_{12}	C_{44}	C_{66}	E_{100}	E_{001}	B	ν_{12}	ν_{13}	ν_{31}
$Fe_{79}Si_{12}B_9$	Present	193.7	233.9	72.1	79.8	63.5	57.0	152.1	195.9	118.3	0.336	0.205	0.264
$Fe_{75}B_{25}$	18	⋯	⋯	⋯	⋯	⋯	⋯	175.5	⋯	⋯	0.32	⋯	⋯
$Fe_{80}B_{20}$	19	⋯	⋯	⋯	⋯	⋯	⋯	165.7	⋯	⋯	⋯	⋯	⋯
$Fe_{80}P_{20}$	19	⋯	⋯	⋯	⋯	⋯	⋯	130.4	⋯	⋯	⋯	⋯	⋯
$Fe_{80}P_{16}C_3B_1$	19	⋯	⋯	⋯	⋯	⋯	⋯	135.3	⋯	⋯	⋯	⋯	⋯

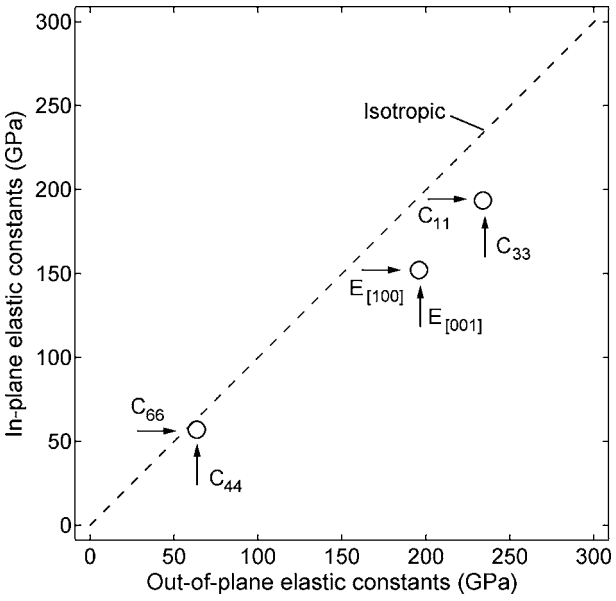

FIG. 5. In-plane and out-of-plane elastic constants of the amorphous alloy thin film. The dashed line in the figure represents the elastic isotropy. The plots are shifted to right side indicating that out-of-plane has high stiffness.

ably soft magnetic property. Denoting the total energy per unit volume to achieve the saturation of magnetization in the in-plane and out-of-plane directions by $E_{\parallel}$ and $E_{\perp}$, respectively, the effective magnetic anisotropy energy E_m can be expressed as follows:

$$E_m = (E_{\perp} - E_{\parallel}) - \frac{N}{2\mu_0} I_s^2, \tag{7}$$

where μ_0 is the vacuum permeability and I_s is the saturation magnetization. N represents the demagnetizing factor and equal unity in the case of a thin film. The last term in Eq. (7) represents the shape magnetic anisotropy energy and calculated to be 8.92×10^5 J/m^3. On the other hand, from Fig. 6, we obtain $E_{\perp} - E_{\parallel} = 7.47 \times 10^5$ J/m^3. The amorphous alloy therefore has a structure dependent magnetic anisotropy (1.45×10^5 J/m^3) between the in-plane and out-of-plane directions.

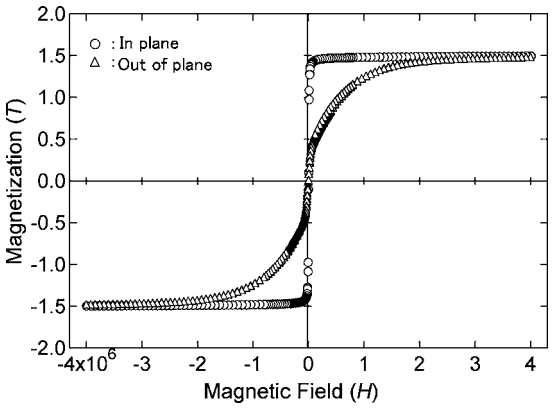

FIG. 6. Magnetic field-magnetization curve of the amorphous alloy thin film obtained by the SQUID at ambient temperature. Open circle and triangle in the figure represent in-plane and out-of-plane measurement. Hysteresis behavior has not been identified indicating the soft magnetic property in both directions.

As originally reported by Bernal,[20,21] and suggested by many researchers,[22] amorphous alloys are known to have short range or medium range orders (SROs, MROs) in their atomic configuration to stabilize amorphous phase at ambient temperature. The $Fe_{79}Si_{12}B_9$ amorphous alloy thin film is expected to have such covalently bonded SRO/MRO clusters since it includes large amount of metalloid elements (Si and P) about 20%. In fact, this tendency can be confirmed from low Poisson's ratio of ν_{13} and ν_{31}; covalently bonded glassy solids (e.g., SiO_2) frequently show low ν.[23] Thus, anisotropy of covalent bonding or equivalently orientational anisotropy of SRO/MRO clusters would exist in the amorphous structure. In the preparation of amorphous alloy thin film, unidirectional solidification to the thickness direction occurs during the quenching process from the liquid state. This solidification process would make local atomic configuration differences between the in-plane and the out-of-plane directions in the orders of SRO or MRO. On the other hand, according to the thermodynamics, adiabatic elastic constants are defined as the second derivative of internal energy with respect to the corresponding uniform strain so that their values are sensitive to the atomic configurations in the amorphous structure. Thus, local atomic configuration differences in the order of SRO/MRO would be one of the reasons for both the elastic and the magnetic anisotropies found in the study.

V. CONCLUSIONS

In conclusion, we have developed an ultrasound spectroscopy technique which determines anisotropic elastic constants of an $Fe_{79}Si_{12}B_9$ amorphous alloy free standing thin film. Out-of-plane shear moduli of C_{44} and C_{55} are determined by the thickness resonance EMAR and showed almost isotropy with a difference of 3%. The consistency of C_{44} and C_{55} suggests that the amorphous alloy thin film has a hexagonal type elastic symmetry. With the assumption, we determined other independent components of C_{ij} by using the modified RUS/LDI technique. In-plane elastic constants of the amorphous alloy thin film showed reasonable values compared with previous works. On the other hand, out-of-plane elastic constants showed weak but finite elastic anisotropies; $C_{33}/C_{11} = 1.21$ and $C_{66}/C_{44} = 1.26$. Magnetization measurements also showed remarkable magnetic anisotropies between the two directions in the amorphous alloy thin film. Short range or medium range ordered anisotropic microstructure would be an origin of the results.

[1] K. Takashima, Y. Higo, S. Sugiura, and M. Shimojo, Mater. Trans. **42**, 68 (2001).
[2] N. L. Rowell and G. I. Stegeman, Phys. Rev. B **18**, 2598 (1978).
[3] A. L. Moretti, W. M. Robertson, B. Fisher, and R. Bray, Phys. Rev. B **31**, 3361 (1985).
[4] P. Djemia, C. Dugautier, T. Chauveau, E. Dogheche, M. I. De Barrors, and L. Vandenbulcke, J. Appl. Phys. **90**, 3771 (2001).
[5] H. Mizubayashi, J. Matsumoto, and H. Tanimoto, Scr. Mater. **41**, 443 (1999).
[6] S. Sakai, H. Tanimoto, and H. Mizubayashi, Acta Mater. **47**, 221 (1999).
[7] T. Malkow, I. A. Garcia, A. Kolitsch, D. Schneiser, S. J. Bull, and T. F. Page, Diamond Relat. Mater. **10**, 2199 (2001).
[8] W. Suwito, M. L. Dunn, S. J. Cunningham, and D. T. Read, J. Appl. Phys. **85**, 3519 (1999).
[9] H. Huang and F. Spaepen, Acta Mater. **48**, 3261 (2000).

[10]D. Faurie, P.-O. Renault, E. Le Bourhis, P. Villain, Ph. Goudeau, and F. Badawi, Thin Solid Films **469–470**, 201 (2004).
[11]A. Migliori, J. Sarrao, J. Visscher, M. W. Bell, T. Lei, M. Fisk, and R. Leisure, Physica B **183**, 1 (1993).
[12]J. H. Demarest, J. Acoust. Soc. Am. **49**, 768 (1971).
[13]I. Ohno, J. Phys. Earth **24**, 355 (1976).
[14]J. Maynard, Phys. Today **49**, 26 (1996).
[15]H. Ledbetter, C. Fortunko, and P. Heyliger, J. Appl. Phys. **78**, 1542 (1995).
[16]M. Hirao and H. Ogi, *EMATs for Science and Industry* (Kluwer Academic, Boston, 2003).
[17]H. Ogi, K. Sato, T. Asada, and M. Hirao, J. Acoust. Soc. Am. **112**, 2553 (2002).
[18]H. S. Chen, Rep. Prog. Phys. **43**, 353 (1980).
[19]L. A. Davis, *Metallic Glasses* (American Society for Metals, Metals Park, OH, 1978).
[20]J. D. Bernal, Nature (London) **183**, 141 (1959); **185**, 68 (1960); J. D. Bernal and J.Mason, *ibid.* **188**, 910 (1960).
[21]J. D. Bernal, Proc. R. Soc. London, Ser. A **280**, 299 (1964).
[22]J. L. Finney, Proc. R. Soc. London, Ser. A **319**, 479 (1970); **319**, 495 (1970).
[23]V. N. Novikov and A. P. Sokolov, Nature (London) **431**, 961 (2004).